

# Stochastic particle method with birth-death dynamics

Zhengyang Lei<sup>a</sup>, Sihong Shao<sup>a</sup>

<sup>a</sup>*CAPT, LMAM and School of Mathematical Sciences, Peking University, Beijing 100871, China*

---

## Abstract

In order to numerically solve high-dimensional nonlinear PDEs and alleviate the curse of dimensionality, a stochastic particle method (SPM) has been proposed to capture the relevant feature of the solution through the adaptive evolution of particles [J. Comput. Phys. 527 (2025) 113818]. In this paper, we introduce an active birth-death dynamics of particles to improve the efficiency of SPM. The resulting method, dubbed SPM-birth-death, sample new particles according to the nonlinear term and execute the annihilation strategy when the number of particles exceeds a given threshold. Preliminary numerical experiments on the Allen-Cahn equation demonstrate that SPM-birth-death can achieve smaller errors at the same computational cost compared with the original SPM.

*Keywords:* Stochastic particle method; Birth-death process; Adaptive sampling; Piecewise constant reconstruction; Allen-Cahn equation

---

## 1. Introduction

With advances in computational mathematics, numerical methods for solving high-dimensional partial differential equations (PDEs) have attracted increasing attention from researchers. Typical high-dimensional PDEs include the 6-D Vlasov equation [1, 2] and the Boltzmann equation [3, 4, 5], which describe the evolution of charged particles in plasma physics, as well as the Hamilton–Jacobi–Bellman equation [6, 7] in control theory, whose dimension is determined by the number of players. The three well-known traditional numerical methods—finite difference, finite element, and spectral methods—are highly mesh-dependent. Consequently, they suffer from the curse of dimensionality (CoD) [6] when applied to high-dimensional PDEs; that is, their computational cost increases exponentially with dimension.

Several numerical attempts have been made to alleviate the CoD, yet these approaches often suffer from limitations and drawbacks. When solutions of high-dimensional PDEs exhibit a low-rank structure, the tensor train method can exploit this structure via low-rank tensor grids, significantly reducing storage costs [8, 9, 7, 10, 11]. However, the effectiveness of this method hinges on the low-rank assumption, which is not always valid, thereby limiting its applicability. The sparse grid method [12, 13, 14] reduces storage requirements by applying a hyperbolic truncation to the tensor product basis set and discarding coefficients with absolute values below a given tolerance. While effective, this coefficient omission can compromise numerical stability [15], and the accuracy is highly sensitive to solution smoothness. Deep-learning-based PDE solvers, currently undergoing rapid development, have been successfully applied to a wide range of high-dimensional problems [16, 17, 18, 19, 20, 21, 22, 23, 24]. However, such solvers exhibit high sensitivity to hyperparameter tuning [25], posing challenges for theoretical understanding [26].

Leveraging the Monte Carlo method’s weak dimensionality dependence, particle methods have emerged as a promising direction for solving high-dimensional problems. Notable examples include:

---

*Email addresses:* [leizy@stu.pku.edu.cn](mailto:leizy@stu.pku.edu.cn) (Zhengyang Lei), [sihong@math.pku.edu.cn](mailto:sihong@math.pku.edu.cn) (Sihong Shao)

the Particle-in-Cell (PIC) method for the Vlasov equation [27, 28, 29], branching random walk algorithms for the Wigner equation [30, 31], and branching diffusion processes for semi-linear parabolic equations [32, 33]. Recently, a stochastic particle method (SPM) was proposed for moderately high-dimensional nonlinear PDEs [34]. This approach simulates solution evolution through particle motion and weight updates while maintaining a constant particle count throughout computation. This paper introduces an SPM incorporating a birth-death mechanism, dubbed SPM-birth-death, that adaptively generates particles in regions requiring enhanced resolution to improve accuracy, and annihilates them in over-resolved areas to boost efficiency.

Prior to this work, particle generation and annihilation mechanisms have been explored in the literature. The hybrid method with deviational particles (HDP) proposed in [35, 36] generates new particles from the source term at each time step and adds them to the original particle system. Consequently, HDP incorporates a particle annihilation mechanism to prevent exponential growth in particle number. This is implemented by first discarding the original particles, followed by resampling a reduced set from the numerical solution. In the Wigner branching random walk algorithm [30, 31], a single particle splits into three upon jumping, while adopting an annihilation strategy that cancels opposing-sign weighted particles within close proximity in phase space. In both methods, particle birth/death constitutes a passive, algorithmically essential component. Critically, the proposed SPM-birth-death actively incorporates a birth-death mechanism into particle methods to enhance computational efficiency. Within plasma simulation PIC methods [27, 28, 29], active particle management strategies have been documented—for instance: splitting heavy-weight particles into light-weight counterparts to maintain accuracy, and merging light-weight particles into heavy-weight ones to reduce computational costs.

The rest of this paper is organized as follows. Section 2 discusses the particle generation and particle annihilation mechanisms and then give SPM-birth-death, while Section 3 conducts numerical experiments to compare SPM-birth-death with SPM. The paper is concluded in Section 4.

## 2. SPM-birth-death

SPM-birth-death adds an active particle birth-death mechanism on the basis of SPM [34]. It inherits the main framework and design ideology of SPM, but differs in the specific particle evolution rules. Consider high-dimensional nonlinear PDEs of the following form

$$\begin{aligned} \frac{\partial}{\partial t} u(\mathbf{x}, t) &= \mathcal{L}u(\mathbf{x}, t) + f(t, \mathbf{x}, u, \nabla u), \quad \mathbf{x} \in \mathbb{R}^d, t > 0, \\ u(\mathbf{x}, 0) &= u_0(\mathbf{x}), \quad \mathbf{x} \in \mathbb{R}^d, \end{aligned} \tag{1}$$

where  $\mathcal{L}$  represents the linear operator,  $f(t, \mathbf{x}, u, \nabla u)$  is the nonlinear term, and the initial data  $u_0(\mathbf{x}) \in L^2(\mathbb{R}^d)$ . Consistent with SPM [34], SPM-birth-death uses the Lawson-Euler scheme [37] to establish the evolution rules of  $u(\mathbf{x}, t)$  in the time direction,

$$U_{m+1}(\mathbf{x}) = e^{\tau \mathcal{L}} (U_m(\mathbf{x}) + \tau f(t_m, \mathbf{x}, U_m, \nabla U_m)), \tag{2}$$

where  $\tau$  is the time step and  $U_m(\mathbf{x})$  denotes the numerical solution at  $t_m = m\tau$ . We use  $N(t)$  stochastic particles to evolve Eq. (2) in the weak sense. In SPM-birth-death, the number of particles  $N(t)$  changes with time, while in SPM,  $N(t) \equiv N(0)$  is maintained. Each particle contains two parameters: the location  $\mathbf{x}_i \in \mathbb{R}^d$  and the weight  $w_i \in \mathbb{R}$ . All particles form a weighted point distribution

$$X_{t_m} := \frac{1}{N(0)} \sum_{i=1}^{N(t_m)} w_i(t_m) \delta_{\mathbf{x}_i(t_m)}, \tag{3}$$

where  $w_i(t_m)$  and  $\mathbf{x}_i(t_m)$  denote the weight and location at time  $t_m$  respectively, and  $\delta$  presents the Dirac distribution. As a result,  $X_{t_m}$  can approximate  $U_m(\mathbf{x})$  in the weak sense

$$\langle \varphi, U_m \rangle \approx \langle \varphi, X_{t_m} \rangle = \frac{1}{N(0)} \sum_{i=1}^{N(t_m)} w_i(t_m) \varphi(\mathbf{x}_i(t_m)), \quad (4)$$

where  $\langle f, g \rangle = \int_{\mathbb{R}^d} f(\mathbf{x})g(\mathbf{x})d\mathbf{x}$  is the standard inner product and the set of test functions is chosen as  $\varphi(\mathbf{x}) = \mathbb{1}_{Q_k}(\mathbf{x}), k = 1, 2, \dots, K$ . The  $\mathbb{1}_{Q_k}(\mathbf{x})$  denotes the indicator function of sub-domain  $Q_k$  and  $\Omega = \bigcup_{k=1}^K Q_k$  constitutes a partition of the computational domain  $\Omega$ . SPM-birth-death designs the evolution rules of the particle system  $X_t$  based on the weak form of the Lawson-Euler scheme

$$\langle \varphi, U_{m+1} \rangle = \langle e^{\tau \mathcal{L}^*} \varphi, U_m + \tau f(t_m, \mathbf{x}, U_m, \nabla U_m) \rangle, \quad (5)$$

where  $\mathcal{L}^*$  is the adjoint operator of the  $\mathcal{L}$  defined on  $\mathbb{H}^2(\mathbb{R}^d)$ .

### 2.1. The birth mechanism

We note that the particle system  $X_{t_m}$  can already approximate  $U_m(\mathbf{x})$  in the weak sense at time  $t_m$ . When the solution evolves from  $U_m(\mathbf{x})$  to  $U_{m+1}(\mathbf{x})$ , it only adds an increment  $\tau f(t_m, \mathbf{x}, U_m, \nabla U_m)$  of order  $\mathcal{O}(\tau)$ , followed by the action of the operator  $e^{\tau \mathcal{L}^*}$ .

Therefore, we can retain the original particle system that can approximate  $U_m(\mathbf{x})$  at  $t_m$ , and then sample a small number of new particles of order  $\mathcal{O}(\tau)$  from

$$p(\mathbf{x}) = \frac{|\tau f(t_m, \mathbf{x}, U_m, \nabla U_m)|}{\int_{\mathbb{R}^d} |\tau f(t_m, \mathbf{x}, U_m, \nabla U_m)| d\mathbf{x}}, \quad (6)$$

and add these new particles to the original particle system. Algorithm 1 presents the detailed process of SPM-birth-death.

In Algorithm 1,  $N(0)$  particles are sampled at the initial moment. At each subsequent time step, we sample  $N_{\text{birth}}$  particles from Eq. (6) with  $N_{\text{birth}} = N(0) \times \tau \int_{\mathbb{R}^d} |f(t_m, \mathbf{x}, U_m, \nabla U_m)| d\mathbf{x}$  (Line 11 in Algorithm 1). The number of newly sampled particles is proportional to  $\tau \int_{\mathbb{R}^d} |f(t_m, \mathbf{x}, U_m, \nabla U_m)| d\mathbf{x}$ , which reflects the effect of the nonlinear term. These new particles are sampled according to the distribution  $\mathbf{x}_i \sim p(\mathbf{x}) = \frac{|\tau f(t_m, \mathbf{x}, U_m, \nabla U_m)|}{\int_{\mathbb{R}^d} |\tau f(t_m, \mathbf{x}, U_m, \nabla U_m)| d\mathbf{x}}$ , and assigned the weight  $w_i = \frac{|\tau f(t_m, \mathbf{x}_i, U_m, \nabla U_m)|}{\tau f(t_m, \mathbf{x}_i, U_m, \nabla U_m)}$  (Lines 11-13 in Algorithm 1). After sampling the new particles, we need to apply the operator  $e^{\tau \mathcal{L}^*}$ . In addition, the updates of  $\mathbf{x}_i$  and  $w_i$  require us to reconstruct the values of  $U_m$  and  $f(t_m, \mathbf{x}, U_m, \nabla U_m)$  from the particle point cloud. In the following, we present the specific implementation of these two aspects, which are consistent with those of SPM [34].

- The linear-operator-guided particle trajectory dynamics: Consider the linear equation,

$$\begin{aligned} \frac{\partial}{\partial t} g(\mathbf{x}, t) &= \mathcal{L}^* g(\mathbf{x}, t), \\ g(\mathbf{x}, 0) &= \varphi(\mathbf{x}), \end{aligned} \quad (7)$$

and it has the formal solution  $g(\mathbf{x}, \tau) = e^{\tau \mathcal{L}^*} \varphi(\mathbf{x})$ , which reflects the action of  $\mathcal{L}^*$ . Here are some simple examples. If  $\mathcal{L} = \mathbf{b} \cdot \nabla$ ,  $\mathbf{b} \in \mathbb{R}^d$  is a constant vector, then  $\mathcal{L}^* = -\mathbf{b} \cdot \nabla$  and the analytical solution of Eq. (7) is

$$e^{\tau \mathcal{L}^*} \varphi(\mathbf{x}) = g(\mathbf{x}, \tau) = \varphi(\mathbf{x} - \mathbf{b}\tau),$$

which implies a kind of linear advection along the characteristic line,

$$\mathbf{x}_i(t_{m+1}) = \mathbf{x}_i(t_m) - \mathbf{b}\tau. \quad (8)$$

If  $\mathcal{L} = c\Delta$ ,  $c$  is a constant, then  $\mathcal{L}^* = c\Delta$ , and the analytical solution of Eq. (7) has the closed form

$$g(\mathbf{x}, \tau) = \int_{\mathbb{R}^d} \frac{1}{(2\pi)^{d/2} \sqrt{|\Sigma|}} e^{-\frac{1}{2}\mathbf{y}^T \Sigma^{-1} \mathbf{y}} \varphi(\mathbf{x} + \mathbf{y}) d\mathbf{y}, \quad \Sigma = 2c\tau \mathbf{I},$$

with  $\mathbf{I}$  is the  $d \times d$  identity matrix. It has a transparent probability interpretation  $e^{c\tau\Delta}\varphi(\mathbf{x}) = \mathbb{E}[\varphi(\mathbf{x} + \mathbf{y})]$ , where  $\mathbf{y}$  obeying the normal distribution  $\mathcal{N}(\mathbf{0}, \Sigma)$ . To be more specific, it relates to the Brownian motion,

$$\mathbf{x}_i(t_{m+1}) = \mathbf{x}_i(t_m) + \mathbf{y}, \quad \mathbf{y} \sim \mathcal{N}(\mathbf{0}, \Sigma). \quad (9)$$

The above shows two examples of local linear operators. For the nonlocal linear operator  $\mathcal{L}$ , the particle motion rules can be designed through the Neumann series expansion [38, 39], and the interested readers can refer to [30, 34] for more details.

- Constructing function values from the point cloud: In the particle evolution at each time step, we need to know the function values of  $U_m(\mathbf{x})$  and  $f(t, \mathbf{x}, U_m(\mathbf{x}), \nabla U_m(\mathbf{x}))$  (see Lines 12 and 13 in Algorithm 1). This involves how to reconstruct  $U_m(\mathbf{x})$  and  $\nabla U_m(\mathbf{x})$  from the particle point cloud (3).

In [34], the so-called virtual uniform grid (VUG) is employed to approximate  $U_m(\mathbf{x})$  by the piecewise constant function. Let  $\Omega = \prod_{j=1}^d [l_j, r_j] \subset \mathbb{R}^d$  denote the computational domain containing all particles. Suppose the particle locations are given by

$$\mathbf{x}_i(t_m) = (x_i^1, x_i^2, \dots, x_i^d), \quad i = 1, 2, \dots, N(t_m), \quad (10)$$

and let  $l_j = \min_{1 \leq i \leq N(t_m)} x_i^j$  and  $r_j = \max_{1 \leq i \leq N(t_m)} x_i^j$ . Then, the computational domain can be decomposed into several grids  $Q_k$  with side length  $h$ ,

$$\Omega = \prod_{j=1}^d [l_j, r_j] = \bigcup_{k=1}^K Q_k. \quad (11)$$

Suppose that the function value at location  $\mathbf{x}$  needs to be estimated, and it lies within the grid  $Q_k$ . Then, based on the weak approximation Eq. (4) of the particle system, we have

$$U_m(\mathbf{x}) \approx \bar{U}_m(\mathbf{x}) = \frac{1}{h^d} \int_{Q_k} U_m(\mathbf{y}) d\mathbf{y} \approx \frac{1}{N(0)} \sum_{i=1}^{N(t_m)} \frac{w_i(t_m) \mathbb{1}_{Q_k}(\mathbf{x}_i(t_m))}{h^d}. \quad (12)$$

In fact, we can derive the second approximation in (12) by substituting the test function  $\varphi(\mathbf{x})$  with the indicator function  $\mathbb{1}_{Q_k}(\mathbf{x})$  in (4). Once the estimation of the function value is obtained, the derivative can be approximated using the central difference quotient. The readers interested in the details can refer to [34]. In terms of storage cost, only the grids  $Q_k$  containing particles need to be stored, as  $U_m(\mathbf{x})$  is approximated as  $\bar{U}_m(\mathbf{x}) = 0$  in grids without particles and thus does not require storage. The dynamic grids generation based on particle locations (instead of full tensor-product grids) is why this method is termed the virtual uniform grid.

Compared with SPM, SPM-birth-death reduces both the computational cost of particle sampling and the errors induced by sampling. At each time step, SPM samples  $N(0)$  particles from

$$\frac{|U_m(\mathbf{x}) + \tau f(t_m, \mathbf{x}, U_m, \nabla U_m)|}{\int_{\mathbb{R}^d} |U_m(\mathbf{x}) + \tau f(t_m, \mathbf{x}, U_m, \nabla U_m)| d\mathbf{x}}. \quad (13)$$

In fact, this is unnecessary because the existing particle system can already approximate the part of  $U_m(\mathbf{x})$ . The SPM-birth-death method only sample a small number of new particles from the  $\mathcal{O}(\tau)$ -order increment, which not only saves the computational cost but also reduces the additional errors introduced by sampling.

## 2.2. The death mechanism

Now we have completed the introduction of the particle generation mechanism, which causes the number of particles to grow exponentially with time during the simulation. Long-term simulations would be unfeasible without a corresponding particle annihilation mechanism to match it. Next, we discuss the particle annihilation mechanism in SPM-birth-death.

In the branching random walk algorithm for the Wigner equation [30, 31], the highly oscillatory nature of the Wigner function causes positive- and negative-weight particles to cluster densely. Consequently, particle annihilation in [31] operates through mutual cancellation of proximal positive/negative-weight particle pairs. For PDE solutions exhibiting weaker oscillations, particle systems typically concentrate positive-weight particles in solution-positive regions and negative-weight particles in solution-negative regions. Notably, PDEs with strictly non-negative solutions may contain no negative-weight particles. This inherent limitation restricts annihilation mechanisms relying on positive-negative cancellation. In [35, 36], particle annihilation is implemented via resampling: Reconstruct the PDE solution from the  $N(t_m)$ -particle ensemble using the Fourier bases; release memory occupied by the original  $N(t_m)$  particles; sample  $N(0)$  new particles from the Fourier-approximated solution; and annihilation occurs when  $N(0) < N(t_m)$ .

SPM-birth-death similarly reduces particle count through resampling with fewer particles. Unlike Fourier basis reconstruction—which employs tensor product structures exhibiting rapid dimensional scaling—our method utilizes the VUG approach [34] for solution reconstruction. VUG capitalizes on particle adaptivity, achieving considerable storage reduction. The complete procedure remains detailed in Algorithm 1 where  $n_A \in (1, +\infty)$ . This algorithm features the parameter  $n_A$  to regulate particle population size. When the particle count  $N(t_m)$  exceeds  $N(0) \times n_A$ , the particle annihilation mechanism is activated: The memory occupied by the original particle system is first released, and then  $N(0)$  particles are sampled based on the piecewise constant approximation of the solution,

$$\begin{aligned} \mathbf{x}_i &\sim \frac{1}{Z} \sum_{k=1}^K |\overline{U}_m(\mathbf{x})| \mathbb{1}_{Q_k}(\mathbf{x}), \quad i = 1, \dots, N(0), \\ w_i &= Z \cdot \frac{\overline{U}_m(\mathbf{x})}{|\overline{U}_m(\mathbf{x})|}, \quad i = 1, \dots, N(0), \end{aligned} \tag{14}$$

where  $Z = \sum_{k=1}^K |\overline{U}_m(\mathbf{x})| h^d$  is the normalization constant.

## 3. Numerical experiments

This section conducts several numerical experiments and makes a comparison between SPM-birth-death and SPM. The two numerical examples below are adopted from [34]. The particle growth threshold parameters in Algorithm 1 is set as  $n_A = 3$  unless otherwise specified.

### 3.1. The 1-D benchmark

We first consider the following 1-D nonlinear model with a Cauchy data to benchmark the two methods,

$$\begin{aligned} \frac{\partial u}{\partial t} &= \nabla u + \Delta u + u - u^3, \\ u(x, 0) &= u_0(x) = \exp(-x^2)(1 + x^4). \end{aligned} \tag{15}$$

---

**Algorithm 1** Stochastic particle method with birth-death dynamics.

---

**Input:** The side length of hypercube  $h$ , the final time  $T$ , the time step  $\tau$ , the particle growth threshold  $n_A$ , the initial data  $u_0(\mathbf{x})$ , the linear operator  $\mathcal{L}$ , the nonlinear term  $f(t, \mathbf{x}, u, \nabla u)$  and the initial partical number  $N(0)$ .

**Output:** The numerical solution to nonlinear PDE (1) at the final time.

```
1: for  $m = 0 : \frac{T-\tau}{\tau}$  do
2:   if  $N(t_m) > N(0) \times n_A$  then
3:     Release the original  $N(t_m)$  particles.
4:     Sample  $N(0)$  particles based on the piecewise constant approximation of  $U_m$  according
   to (14);
5:      $N(t_m) \leftarrow N(0)$ ;
6:   end if
7:   if  $m = 0$  then
8:     Sample  $\mathbf{x}_i$  from  $p(\mathbf{x}) = \frac{|U_0(\mathbf{x})|}{\int_{\mathbb{R}^d} |U_0(\mathbf{x})| d\mathbf{x}}$ ,  $i = 1, \dots, N(0)$ ;
9:      $w_i \leftarrow \frac{U_0(\mathbf{x}_i)}{p(\mathbf{x}_i)}$ ,  $i = 1, \dots, N(0)$ ;
10:  end if
11:  Compute the particle number to be generated  $N_{\text{birth}} \leftarrow N(0) \times \tau \int_{\mathbb{R}^d} |f(t_m, \mathbf{x}, U_m, \nabla U_m)| d\mathbf{x}$ ;
12:  Sample new particles  $\mathbf{x}_i$  from  $p(\mathbf{x}) = \frac{|\tau f(t_m, \mathbf{x}, U_m, \nabla U_m)|}{\int_{\mathbb{R}^d} |\tau f(t_m, \mathbf{x}, U_m, \nabla U_m)| d\mathbf{x}}$ ,  $i = N(t_m) + 1, \dots, N(t_m) +$ 
   $N_{\text{birth}}$ ;
13:   $w_i \leftarrow \frac{|\tau f(t_m, \mathbf{x}_i, U_m, \nabla U_m)|}{\tau f(t_m, \mathbf{x}_i, U_m, \nabla U_m)}$ ,  $i = N(t_m) + 1, \dots, N(t_m) + N_{\text{birth}}$ ;
14:   $N(t_{m+1}) \leftarrow N(t_m) + N_{\text{birth}}$ ;
15:  Move particle according to  $\mathcal{L}^*$ ;
16:  Obtain the piecewise constant approximation of  $U_{m+1}$  and  $f(t_{m+1}, \mathbf{x}, U_{m+1}, \nabla U_{m+1})$  based
  on the virtual uniform grid;
17: end for
```

---

The relative  $L^2$  error

$$\mathcal{E}_2[u](t) = \frac{\|u^{\text{num}}(x, t) - u^{\text{ref}}(x, t)\|_2}{\|u^{\text{ref}}(x, t)\|_2} \quad (16)$$

is employed to measure the accuracy. The reference solutions  $u^{\text{ref}}$  to Eq. (16) are produced by a deterministic solver which adopts the second-order operator splitting [40]. The 1-D benchmark in this section are implemented via Matlab with platform parameters: Intel (R) Core (TM) i7-6700 CPU (3.40 GHz), 16.0 GB of memory. We set the final time  $T = 10$ , the time step  $\tau = 0.1$  and the side length of hypercube  $h = 0.1$  in Algorithm 1 unless otherwise indicated.

Table 1 demonstrates the convergence order of SPM-birth-death. As expected, the method achieves half-order accuracy with respect to initial sample size  $N(0)$ . Due to its Lawson-Euler scheme and piecewise constant reconstruction, it exhibits first-order convergence in both time step  $\tau$  and spatial resolution  $h$ . Figure 1 reveals systematic accuracy improvement under SPM-birth-death, with solution variance decreasing as  $N(0)$  increases. Figure 2 illustrates the particle annihilation mechanism for different  $n_A$  parameters: Particles are annihilated when the count exceeds  $n_A \times N(0)$ , reducing computational costs. Figure 3 confirms SPM-birth-death's superior computational efficiency versus the standard SPM [34], achieving lower errors at equivalent computational costs.

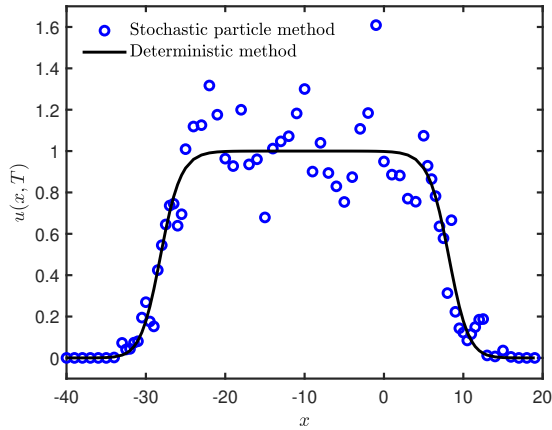
### 3.2. The $d$ -D Allen-Cahn equation

Next we consider the high-dimensional numerical experiments with the  $d$ -D Allen-Cahn equation,

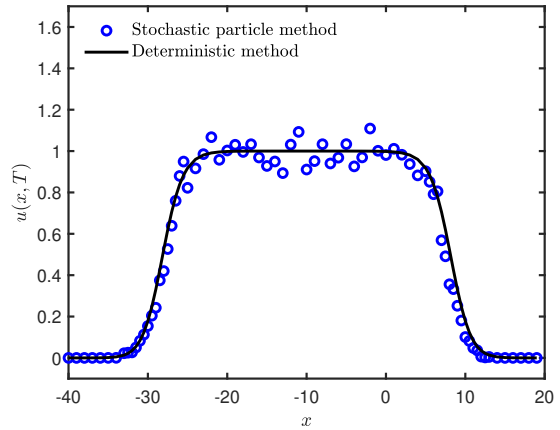
$$\frac{\partial}{\partial t} u(\mathbf{x}, t) = c\Delta u(\mathbf{x}, t) + u(\mathbf{x}, t) - u^3(\mathbf{x}, t) + r(\mathbf{x}, t), \quad \mathbf{x} \in \mathbb{R}^d, \quad (17)$$

Table 1. 1-D benchmark: SPM-birth-death has first-order accuracy in both time and space plus half-order accuracy in the initial sample size.

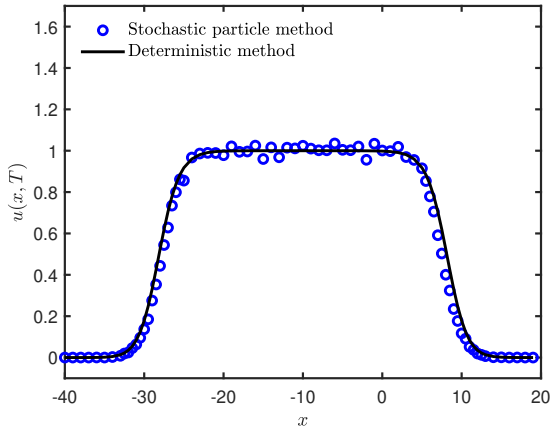
$N(0)$	$h$	$\tau$	$\mathcal{E}_2[u](10)$	order
$1 \times 10^4$			0.5783	-
$4 \times 10^4$	0.01	0.01	0.2988	0.48
$1.6 \times 10^5$			0.1504	0.49
		0.25	0.1023	-
$1 \times 10^7$	0.01	0.2	0.0809	1.05
		0.1	0.0414	0.99
	0.2		0.0106	-
$1 \times 10^7$	0.15	0.01	0.0076	1.15
	0.1		0.0051	1.05



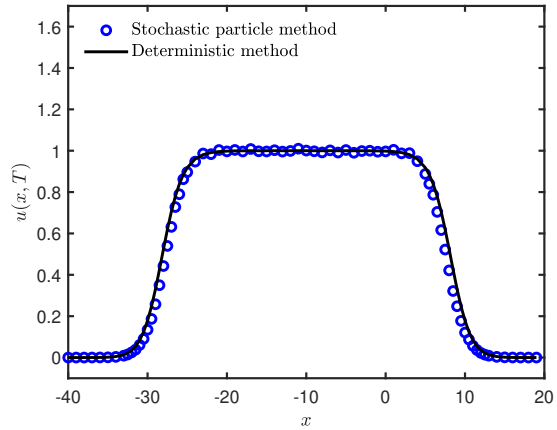
(a)  $N(0) = 1 \times 10^4$ , SPM-birth-death.



(b)  $N(0) = 1 \times 10^5$ , SPM-birth-death.



(c)  $N(0) = 1 \times 10^6$ , SPM-birth-death.



(d)  $N(0) = 1 \times 10^7$ , SPM-birth-death.

Figure 1. 1-D benchmark: The numerical effects of SPM-birth-death with different particle numbers show that its variance decreases as the initial sampling number  $N(0)$  increases.

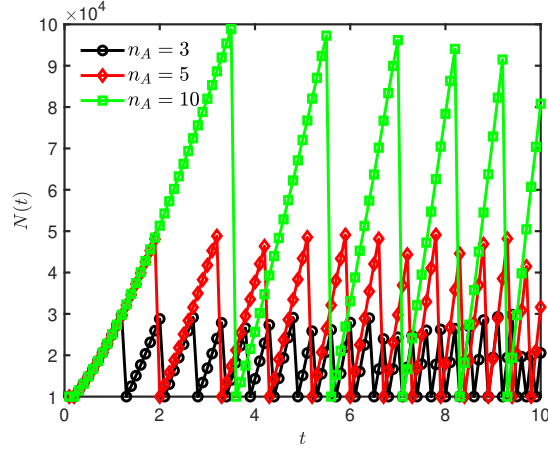


Figure 2. 1-D benchmark: The variation of particle number over time for SPM-birth-death. When the particle number surpasses  $n_A \times N(0)$ , the particle annihilation mechanism is activated, resulting in a reduction of the particle number.

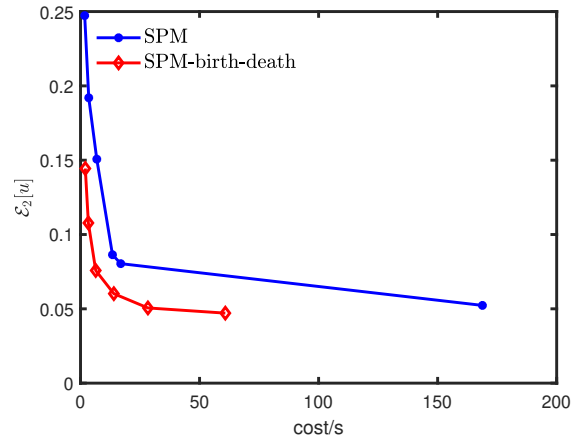


Figure 3. 1-D benchmark: The correlation between relative  $L^2$  error  $\mathcal{E}_2[u]$  and computational cost for SPM and SPM-birth-death. SPM-birth-death demonstrates superior computational efficiency: achieving lower errors at equivalent computational times and requiring shorter times to reach equivalent error levels. We set in SPM:  $N(0) = 1 \times 10^5, 2 \times 10^5, 4 \times 10^5, 8 \times 10^5, 1 \times 10^6, 1 \times 10^7$  with the corresponding running time respectively being 1.7502, 3.4546, 6.8315, 13.42, 16.8924, 168.81 seconds, and in SPM-birth-death:  $N(0) = 2 \times 10^4, 4 \times 10^4, 8 \times 10^4, 2 \times 10^5, 4 \times 10^5, 8 \times 10^5$  with the corresponding running time respectively being 2.0102, 3.2941, 6.3855, 13.9954, 28.31, 60.82 seconds. Here sample sizes were strategically selected to ensure comparable runtimes, enabling direct comparison within the same figure.

which allows the following analytical solution

$$u^{\text{ref}}(\mathbf{x}, t) = \frac{x_1 + x_2}{(\pi(1 + 4ct))^{d/2}} \left( \exp\left(-\frac{\|\mathbf{x} - \mathbf{p}_1\|_2^2}{1 + 4ct}\right) + 2.0 \exp\left(-\frac{\|\mathbf{x} - \mathbf{p}_2\|_2^2}{1 + 4ct}\right) \right), \quad (18)$$

where  $\mathbf{p}_1 = (2, 2, 0, \dots, 0)$ ,  $\mathbf{p}_2 = (-1, -1, 0, \dots, 0)$  and  $c = 1$  is the diffusion coefficient. The initial data  $u_0(\mathbf{x}) = u^{\text{ref}}(\mathbf{x}, 0)$  and let  $r(\mathbf{x}, t)$  be the remaining term after substituting the analytical solution Eq. (18) into Eq. (17). We set the final time  $T = 2$ , the time step  $\tau = 0.1$  and the side length of hypercube  $h = 0.4$  in Algorithm 1 unless otherwise specified. To visualize high-dimensional solutions, we adopt the following 2-D projection,

$$M(x_1, x_2, t) = \int_{\mathbb{R}^{d-2}} u(\mathbf{x}, t) dx_3 \dots dx_d, \quad (19)$$

and use the relative  $L^2$  error  $\mathcal{E}[M](t)$  to measure the accuracy. The 2-D projection is approximated by a uniform partition (take test function  $\varphi(\mathbf{x}) = \mathbb{1}_{Q^\mu \times Q^\nu}$ ),

$$M(x_1, x_2, t) \approx \sum_{\mu=1}^{(r_1-l_1)/h} \sum_{\nu=1}^{(r_2-l_2)/h} \left( \frac{1}{N(t)|Q^\mu||Q^\nu|} \sum_{i=1}^{N(t)} w_i(t) \mathbb{1}_{Q^\mu \times Q^\nu}(\mathbf{x}_i(t)) \right) \mathbb{1}_{Q^\mu \times Q^\nu}(x_1, x_2), \quad (20)$$

where  $Q^\mu = [l_1 + (\mu - 1)h, l_1 + \mu h]$ ,  $Q^\nu = [l_2 + (\nu - 1)h, l_2 + \nu h]$ . The simulations in this section via our C++ implementations run on the High-Performance Computing Platform of Peking University: 2\*Intel Xeon E5-2697A-v4 (2.60 GHz, 40 MB Cache, 9.6GT/s QPI Speed, 16 Cores, 32 Threads) with 256 GB Memory  $\times$  16. Figure 4 plots  $M(x_1, x_2, 2)$  defined in Eq. (19) produced by SPM-birth-death with  $N(0) = 1 \times 10^8$  against the reference solution given in Eq. (18). The agreement between them is evident. The characteristic of moving with the solution for particle locations in SPM-birth-death is clearly demonstrated in the last plot of Figure 4. Figure 5 shows a comparison of the computational efficiency between SPM and SPM-birth-death in the high-dimensional example. Similar to the 1-D benchmark tests, SPM-birth-death is more efficient than SPM owing to the birth-death mechanism.

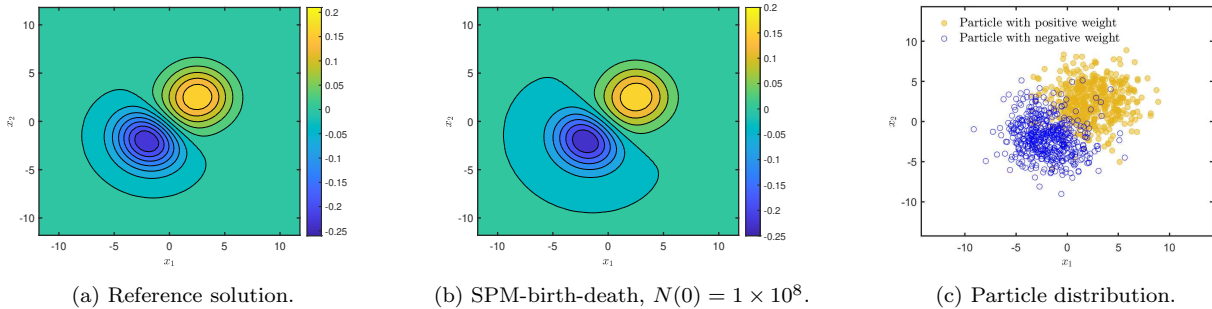


Figure 4. The 6-D Allen-Cahn equation: Filled contour plots of  $M(x_1, x_2, 2)$  defined in Eq. (19) for (a) the reference solution given in Eq. (18) and (b) the numerical solution produced by SPM-birth-death with  $N(0) = 1 \times 10^8$ . We randomly choose  $10^3$  particles from all samples at the final instant  $T = 2$  and project their locations onto the  $x_1x_2$ -plane in (c) to show that the particles in SPM-birth-death exhibit highly adaptive characteristic. The particles with positive and negative weights concentrate in the areas where the solution takes positive and negative values, respectively.

## 4. Conclusion and discussion

The primary contribution of this work is the proposal of SPM-birth-death—a method that inherits the core framework and design philosophy of SPM [34] but incorporates an active particle

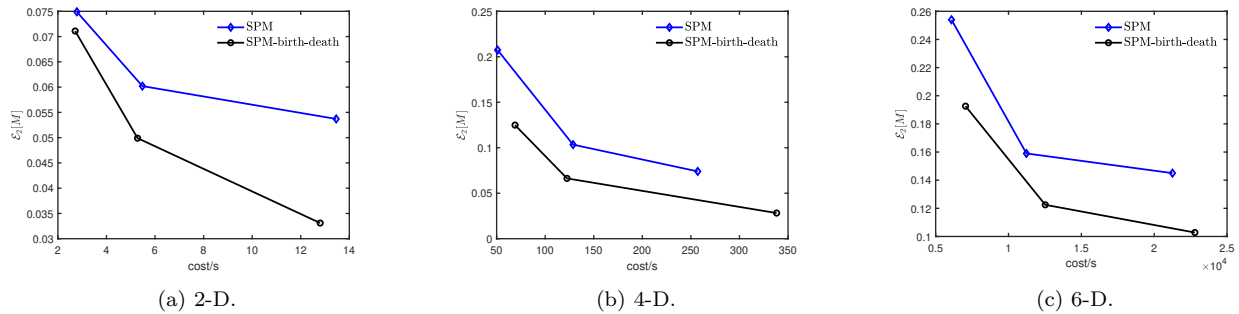


Figure 5. The d-D Allen-Cahn equation: The relationship between relative  $L^2$  error  $\mathcal{E}_2[M]$  and computational time cost for SPM and SPM-birth-death in different dimensions. Compared with SPM, SPM-birth-death can achieve smaller errors at the same computational cost in various dimensions. By selecting different sample sizes in the two methods to ensure comparable running times, we can plot their results in the same figure. Here we set the side length of hypercube  $h = 0.3$  in 2-D and 4-D experiments.

birth-death mechanism to enhance computational efficiency. Numerical experiments across one-dimensional and high-dimensional settings demonstrate SPM-birth-death’s superior accuracy over standard SPM at equivalent computational costs. Several aspects remain open for exploration, including: (i) alternative birth-death strategies, (ii) more efficient methods for function reconstruction from particle clouds, and (iii) rigorous quantitative error analysis for birth-death enhanced SPM dynamics.

## Acknowledgement

This research was supported by the National Natural Science Foundation of China (Nos. 12325112, 12288101) and the High-performance Computing Platform of Peking University.

## References

- [1] K. Kormann, K. Reuter, M. Rampp, A massively parallel semi-Lagrangian solver for the six-dimensional Vlasov-Poisson equation, *International Journal of High Performance Computing Applications* 33 (2019) 924–947.
- [2] A. A. Vlasov, *Many-Particle Theory and Its Application to Plasma*, Gordon and Breach, 1961.
- [3] G. Dimarco, R. Loubère, J. Narski, T. Rey, An efficient numerical method for solving the Boltzmann equation in multidimensions, *Journal of Computational Physics* 353 (2018) 46–81.
- [4] G. A. Bird, Direct simulation and the Boltzmann equation, *Physics of Fluids* 13 (1970) 2676–2681.
- [5] C. Cercignani, *The Boltzmann Equation and its Applications*, Springer, 1988.
- [6] R. E. Bellman, *Dynamic Programming*, Princeton University Press, 1957.
- [7] S. Dolgov, D. Kalise, K. K. Kunisch, Tensor decomposition methods for high-dimensional Hamilton-Jacobi-Bellman equations, *SIAM Journal on Scientific Computing* 43 (2021) A1625–A1650.
- [8] M. Bachmayr, Low-rank tensor methods for partial differential equations, *Acta Numerica* 32 (2023) 1–121.

- [9] M. Bachmayr, R. Schneider, A. Uschmajew, Tensor networks and hierarchical tensors for the solution of high-dimensional partial differential equations, *Foundations of Computational Mathematics* 16 (2016) 1423–1472.
- [10] X. Tang, L. Ying, Solving high-dimensional Fokker-Planck equation with functional hierarchical tensor, *Journal of Computational Physics* 511 (2024) 113110.
- [11] L. Richter, L. Sallandt, N. Nüsken, From continuous-time formulations to discretization schemes: tensor trains and robust regression for BSDEs and parabolic PDEs, *Journal of Machine Learning Research* 25 (2024) 1–40.
- [12] H.-J. Bungartz, M. Griebel, Sparse grids, *Acta Numerica* 13 (2004) 147–269.
- [13] M. Griebel, M. Schneider, C. Zenger, A combination technique for the solution of sparse grid problems, *Forschungsberichte, TU Munich* (1990) 1–24.
- [14] M. Griebel, J. Hamaekers, Sparse grids for the schrödinger equation, *ESAIM: Mathematical Modelling and Numerical Analysis* 41 (2007) 215–247.
- [15] K. Kormann, E. Sonnendrücker, Sparse grids for the Vlasov-Poisson equation, in: *Sparse Grids and Applications-Stuttgart 2014*, Springer, 2016, pp. 163–190.
- [16] J. Han, A. Jentzen, W. E, Solving high-dimensional partial differential equations using deep learning, *Proceedings of the National Academy of Sciences* 115 (2018) 8505–8510.
- [17] M. Raissi, P. Perdikaris, G. E. Karniadakis, Physics-informed neural networks: A deep learning framework for solving forward and inverse problems involving nonlinear partial differential equations, *Journal of Computational Physics* 378 (2019) 686–707.
- [18] C. Huré, H. Pham, X. Warin, Deep backward schemes for high-dimensional nonlinear PDEs, *Mathematics of Computation* 89 (2020) 1547–1579.
- [19] W. E, C. Ma, L. Wu, Machine learning from a continuous viewpoint, I, *Science China Mathematics* 63 (2020) 2233–2266.
- [20] J. Sirignano, K. Spiliopoulos, DGM: A deep learning algorithm for solving partial differential equations, *Journal of Computational Physics* 375 (2018) 1339–1364.
- [21] W. E, B. Yu, The deep ritz method: A deep learning-based numerical algorithm for solving variational problems, *Communications in Mathematics and Statistics* 6 (2018) 1–12.
- [22] Z. Li, N. Kovachki, K. Azizzadenesheli, B. Liu, A. Stuart, A. Anandkumar, Fourier neural operator for parametric partial differential equations, in: *International Conference on Learning Representations*, 2021.
- [23] L. Lu, P. Jin, G. E. Karniadakis, Learning nonlinear operators via DeepONet based on the universal approximation theorem of operators, *Nature Machine Intelligence* 3 (2021) 218–229.
- [24] S. Zeng, Z. Zhang, Q. Zou, Adaptive deep neural networks methods for high-dimensional partial differential equations, *Journal of Computational Physics* 463 (2022) 111232.
- [25] M. Kast, J. S. Hesthaven, Positional embeddings for solving PDEs with evolutionary deep neural networks, *Journal of Computational Physics* 508 (2024) 112986.
- [26] L. Richter, L. Sallandt, N. Nüsken, Solving high-dimensional parabolic PDEs using the tensor train format, in: *Proceedings of the 38th International Conference on Machine Learning*, 2021, pp. 8998–9009.

- [27] Y. Chen, G. Tóth, H. Zhou, X. Wang, Fleks: A flexible particle-in-cell code for multi-scale plasma simulations, *Computer Physics Communications* 287 (2023) 108714.
- [28] P. T. Luu, T. Tückmantel, A. Pukhov, Voronoi particle merging algorithm for PIC codes, *Computer Physics Communications* 202 (2016) 165–174.
- [29] J. Teunissen, U. Ebert, Controlling the weights of simulation particles: adaptive particle management using k-d trees, *Journal of Computational Physics* 259 (2014) 318–330.
- [30] S. Shao, Y. Xiong, Branching random walk solutions to the Wigner equation, *SIAM Journal on Numerical Analysis* 58 (2020) 2589–2608.
- [31] Y. Xiong, S. Shao, Overcoming the numerical sign problem in the Wigner dynamics via adaptive particle annihilation, *SIAM Journal on Scientific Computing* 46 (2024) B107–B136.
- [32] H. L. Pierre, O. Nadia, X. Tan, N. Touzi, X. Warin, Branching diffusion representation of semilinear PDEs and Monte Carlo approximation, *Annales de l’institut Henri Poincaré (B) Probability and Statistics* 55 (2019) 184–210.
- [33] A. J. Chorin, O. H. Hald, *Stochastic Tools in Mathematics and Science*, volume 1, Springer, 2009.
- [34] Z. Lei, S. Shao, Y. Xiong, An efficient stochastic particle method for moderately high-dimensional nonlinear pdes, *Journal of Computational Physics* 527 (2025) 113818.
- [35] B. Yan, R. E. Caflisch, A Monte Carlo method with negative particles for Coulomb collisions, *Journal of Computational Physics* 298 (2015) 711–740.
- [36] B. Yan, A hybrid method with deviational particles for spatial inhomogeneous plasma, *Journal of Computational Physics* 309 (2016) 18–36.
- [37] J. D. Lawson, Generalized Runge-Kutta processes for stable systems with large Lipschitz constants, *SIAM Journal on Numerical Analysis* 4 (1967) 372–380.
- [38] W. Rudin, *Functional Analysis*, McGraw-Hill, 1991.
- [39] R. Kress, *Linear Integral Equations*, Springer, 2014.
- [40] E. Hansen, F. Kramer, A. Ostermann, A second-order positivity preserving scheme for semi-linear parabolic problems, *Applied Numerical Mathematics* 62 (2012) 1428–1435.